Sound & Vibration 2026, 60(4), 4280.
doi: https://doi.org/10.59400/sv4280

Article

Nonlinear sloshing dynamics in rigid cylindrical shells under combined horizontal and vertical excitation

Elena Strelnikova[1,2,3*], Andrii Rusanov[1], Vasyl Gnitko[1], Kyrylo Degtyariov[1,2], Denys Kriutchenko[1], Andrii Kolodiazhnyi[1], Demyd Sinchenko[1]

[1] A N. Pidhorny Institute of Power Machines and Systems, Ukrainian Academy of Sciences, 61023 Kharkov, Ukraine
[2] Computer Physics and Energy Department, V.N. Karazin Kharkiv National University, 61022 Kharkiv, Ukraine
[3] Applied Mathematics Department, Kharkiv National University of Radio Electronics, 61166 Kharkov, Ukraine
*** Corresponding author:** Elena Strelnikova, elena15@gmx.com or Olena.Strelnikova@nure,us

CITATION

Strelnikova E, Rusanov A, Gnitko V, et al. Nonlinear sloshing dynamics in rigid cylindrical shells under combined horizontal and vertical excitation. Sound & Vibration. 2026; 60(4): 4280. https://doi.org/10.59400/sv4280

ARTICLE INFO

Received: 15 April 2026
Revised: 21 May 2026
Accepted: 27 May 2026
Available online: 21 July 2026

Abstract: This paper presents the theoretical foundations for the nonlinear modelling of liquid sloshing dynamics in shells of revolution subjected to combined horizontal and vertical excitations. The proposed mathematical model integrates a spectral approach, the boundary element method (BEM), and a modal representation of the solution in generalized coordinates. This unified framework enables consistent analysis of both linear and nonlinear sloshing phenomena. The spectral boundary-value problem is reduced to a system of singular integral equations defined on the free and wetted surfaces of the shell. The 2π-periodicity of the integral operators is rigorously established, and the structure of the kernel singularities is identified. This ensures mathematical consistency and supports efficient numerical implementation. Natural sloshing modes and frequencies are computed using a BEM-based solver. Based on these eigenmodes, a modal expansion is constructed, leading to reduced-order systems of nonlinear ordinary differential equations. Governing equations are derived for both linear and nonlinear formulations, allowing detailed investigation of sloshing responses under simultaneous horizontal and vertical excitations. Rayleigh damping is incorporated into the modal system; its applicability and physical justification are discussed, along with its limitations in capturing energy dissipation in violent sloshing processes. Numerical results for rigid cylindrical shells illustrate the significant influence of nonlinear modal interactions and combined loading on free-surface elevation. The developed approach provides an effective tool for predicting complex sloshing behaviour beyond the capabilities of purely linear theory.

Keywords: liquid-filled tanks; nonlinear sloshing; spectral boundary problem; singular integral equations; Rayleigh damping; resonance phenomena

1. Introduction

Liquid sloshing in partially filled tanks is a critical phenomenon in aerospace, marine, civil, and nuclear engineering applications, including ship stability, LNG carriers, spacecraft fuel tanks, and the seismic design of storage reservoirs. Linear potential-flow theories adequately describe small-amplitude motions near the fundamental natural frequency; however, they fail to capture essential nonlinear effects that become dominant under large excitations, near-resonant conditions, or in complex geometries [1]. These nonlinear effects include higher-harmonic generation, wave breaking, swirling (rotary) motions, hydraulic jumps, internal resonances, parametric instabilities, chaotic behaviour, and strong fluid–structure interaction. Accurate prediction of free-surface elevations, hydrodynamic pressures, forces, and moments therefore requires advanced analytical (modal and asymptotic), numerical (CFD, FEM, BEM), and experimental approaches.

Foundational studies on nonlinear sloshing date back to the 1950s–1970s. Abramson et al. [2] conducted extensive experimental investigations of nonlinear lateral sloshing in rigid tanks of various geometries, demonstrating a decrease in response frequency with increasing excitation amplitude, as well as "jump" phenomena that cannot be predicted by linear theory. Faltinsen [3] developed one of the first nonlinear analytical models for two-dimensional sloshing in rectangular tanks using perturbation methods for small but finite amplitudes. This work was extended in Liu et al. [4], where a numerical nonlinear potential-flow formulation was proposed that satisfies the exact nonlinear free-surface boundary conditions.

A major advancement in analytical modelling was achieved through multimodal (modal expansion) techniques. Faltinsen et al. [5] derived a general infinite-dimensional modal system for nonlinear sloshing in rectangular tanks with finite liquid depth, without imposing small-amplitude assumptions. This approach was further refined by Faltinsen and Timokha [6] with including an adaptive multimodal framework that systematically truncates higher-order modes while preserving the ability to capture secondary resonances and maintaining accuracy across a wide range of filling levels. In Faltinsen and Timokha [7], these methods were used for various tank geometries and excitation types. Ibrahim in [1] provided an extensive review of both linear and nonlinear theories, including parametric sloshing, Faraday waves, and interactions with elastic containers, with particular emphasis on nonlinear coupling and damping mechanisms.

Subsequent research extended these approaches to specific configurations and excitation types. Zhang et al. [8] developed nonlinear viscous models of sloshing in moving rectangular tanks. Ikeda et al. [9] investigated nonlinear responses in square tanks under oblique horizontal excitation, revealing a strong 1:1 internal resonance between dominant modes. Gavrilyuk et al. [10] and related studies [11–13] applied multimodal techniques to circular, conical, and cylindrical tanks.

Recent extensions of multimodal approaches have addressed viscous effects and practical limitations of purely inviscid models. For instance, Miliaiev and Timokha [14] investigated viscous damping of steady-state resonant sloshing in clean rectangular tanks, providing refined quantification of boundary-layer and bulk damping that improves amplitude-dependent predictions where classical inviscid multimodal theories (e.g., Lukovsky–Timokha frameworks [11–13]) rely on phenomenological adjustments.

In recent decades, research has increasingly focused on fully nonlinear numerical simulations capable of capturing violent sloshing, wave impacts, and complex geometries where analytical models are no longer applicable. Recent reviews (e.g., Konar and Das [15] and Zhang et al. [16]) highlight the state of the art: mesh-based methods (FEM, FVM, BEM), combined with interface-capturing techniques (VOF, Level-Set), as well as meshless particle methods (SPH, MPS), are essential for modelling large-amplitude sloshing. Arbitrary Lagrangian–Eulerian (ALE) FEM formulations, as demonstrated by Ma et al. [17], enable accurate simulation of nonlinear sloshing in non-standard tank geometries, e.g., Cassini or ellipsoidal shapes. Semi-analytical and hybrid approaches [13, 18] offer a compromise between computational efficiency and accuracy, particularly for baffled tanks or seismic loading conditions.

Recent reviews, such as Konar and Das [15], provide a comprehensive state-of-the-art overview of mesh-based (FDM, FEM, FVM), mesh-free (SPH), and hybrid methods, highlighting assumptions and limitations (e.g., mesh distortion in violent sloshing), and applicability domains.

Semi-analytical and hybrid modal methods continue to evolve for baffled tanks and specific excitations, offering a balance between efficiency and accuracy. Meng et al. [19] developed a nonlinear semi-analytical scheme for finite-amplitude sloshing in horizontally baffled rectangular containers under seismic excitation, extending multimodal expansions to incorporate baffle-induced dissipation and modified wave patterns. Similarly, Cao et al. [18] employed a Multi-Domain Eigenvalue Matching (MDEM) method combined with multimodal theory to study nonlinear sloshing in rectangular tanks with vertical baffles, revealing enhanced wave reflections, accelerated transitions to chaotic regimes at higher baffle positions, and improved suppression characteristics.

Seismic applications further emphasise the practical importance of nonlinear effects. Barik and Biswal [20] and Roy and Biswal [21] employed nonlinear finite-element models to analyse sloshing in base-isolated and chamfered-bottom tanks subjected to near- and far-fault earthquakes, demonstrating that free-surface nonlinearity significantly influences both convective and impulsive pressure components, as well as base shear. Baffles and submerged structures are commonly investigated as passive damping devices, with their efficiency strongly governed by nonlinear flow effects [22,23].

Barik and Biswal [24] conducted nonlinear seismic analysis of base-isolated liquid storage tanks with internal blocks using coupled Eulerian-Lagrangian FEM, demonstrating that nonlinear free-surface effects lead to higher amplitudes compared to linear models, while isolation combined with blocks effectively reduces pressures and base shear

Brietman et al. [25] proposed robust finite-element procedures for 2D/3D nonlinear potential-flow sloshing with advanced post-processing (digital filters) for accurate wave elevations and pressures.

The multimodal approach has also been successfully applied to more complex support conditions. Limarchenko et al. [26] investigated the manifestation of secondary (internal) resonances in a tank with liquid suspended as a physical pendulum. Using a nonlinear multimodal model, they demonstrated that for short and medium pendulum lengths, the dominant antisymmetric mode is excited not only at its natural frequency but also at frequencies arising from nonlinear energy transfer between modes. This highlights the importance of accounting for modal coupling even under relatively mild pendulum-type excitations

Experimental validation remains indispensable. Many recent studies, e.g., Ma et al. [17], Hu et al. [23], Yoshitake et al. [27] combine high-fidelity numerical simulations with scaled experiments to quantify discrepancies arising from viscosity, air entrapment, and scale effects, particularly in violent sloshing regimes.

Overall, the literature demonstrates a clear evolution: from weakly nonlinear perturbation and modal methods suitable for moderate amplitudes to high-fidelity CFD and hybrid approaches capable of resolving strong nonlinearities, wave breaking, and multiphysics coupling. Nevertheless, several challenges remain, including full-scale validation, hydroelastic effects in flexible tanks, multi-layer fluid systems, and real-time prediction for control applications. Future research directions include AI-enhanced modelling, improved turbulence modelling (LES/RANS), and tighter integration of nonlinear sloshing dynamics with vessel motion to ensure safer and more efficient tank design.

In addition to problem-specific sloshing models, a wide class of numerical methods for boundary-value problems in continuum mechanics has been successfully applied to sloshing analysis. In particular, the finite element method (FEM), boundary element method (BEM), and finite volume method (FVM) provide versatile frameworks for solving the governing equations with complex geometries, boundary conditions, and multiphysics coupling [28–30].

The FEM is widely used due to its flexibility in handling irregular domains and its natural extension to fluid–structure interaction problems [31]. The BEM is especially efficient for potential-flow formulations, as it reduces the problem dimensionality by one and is well suited for free-surface problems in inviscid fluids [32, 33]. The FVM, commonly employed in CFD, ensures strict conservation properties and is particularly effective for strongly nonlinear flows with moving interfaces when combined with interface-capturing techniques such as VOF or Level-Set methods [34].

These methods form the computational backbone of modern sloshing simulations and enable accurate prediction of nonlinear free-surface dynamics, hydrodynamic loads, and wave impacts in engineering applications. Their development and integration with advanced turbulence models and adaptive meshing techniques continue to expand the range of tractable sloshing problems.

Despite significant progress, challenges remain in the modelling of hydro-elastic effects, multi-layer fluids, and full-scale validation, as well as in the development of reduced-order models suitable for real-time applications. Future research is expected to focus on improved turbulence modelling, hybrid computational frameworks, and data-driven approaches for enhanced predictive capability.

In summary, the proposed nonlinear spectral method occupies an intermediate position between low-order asymptotic models and high-fidelity CFD. It offers a useful tool for studying resonant liquid sloshing and associated vibrations, provided its limitations regarding viscous effects and wave breaking are respected.

2. General formulation of a nonlinear boundary-value problem

The vibrations of a fluid in rigid reservoirs are studied. The problem formulation is based on the classical assumptions of hydrodynamics. A rigid reservoir is considered, partially filled with a liquid (density ρ ≈ 997 kg/m^3), above which there is a gas phase (air) at a constant atmospheric pressure. The influence of surface tension forces is not taken into account, as for water at room temperature (ρ ≈ 1,000 kg/m^3, g ≈ 9.81 m/s^2, σ ≈ 0.072 N/m, characteristic dimension L ≈ 0.5 m), the Bond number is Bo = ρgL^2/σ ≈ 3.5 × 10^4, which indicates the dominance of gravitational forces over surface tension forces. The free surface is idealized without taking into account phase transitions, in particular evaporation and condensation. Dynamic effects in the gas phase, including compressibility, internal flows, and pressure fluctuations, are not considered. The fluid is assumed to be isothermal, and thermal effects are ignored, which is acceptable in the absence of external heat sources. Viscous effects are limited to thin boundary layers and do not significantly affect the natural frequencies and mode shapes, which justifies the use of the potential flow model as a standard first-approximation approach.

In Raynovskyy and Timokha [35] and Fang et al. [36], it was established that the lowest natural frequencies of the "shell-fluid" system correspond to the oscillations of the free surface of the fluid in a rigid shell. In Fang et al. [36], conditions are also given under which the mutual influence of elastic wall vibrations and free surface sloshing cannot be neglected; however, such conditions occur in the case of very thin shells. In this regard, rigid shells partially filled with fluid are further considered (**Figure 1**).

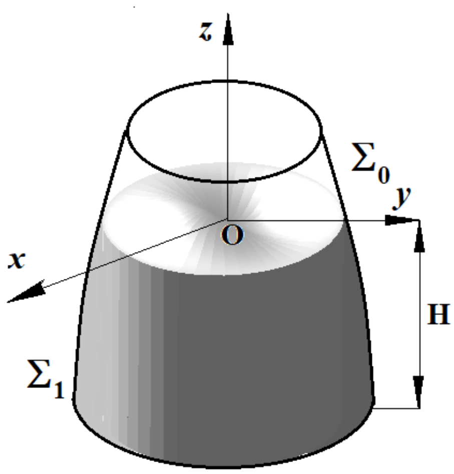

(a)

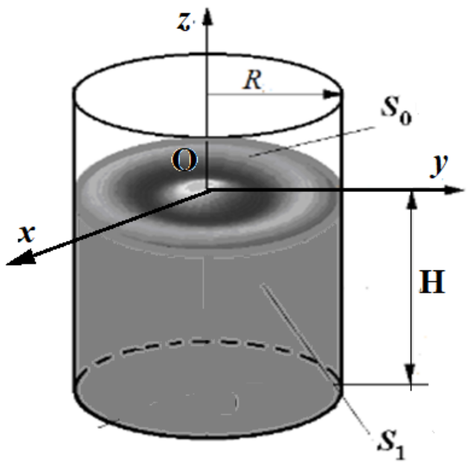

(b)

Figure 1. A rigid shell of revolution partially filled with liquid: **(a)** Arbitrary shell of revolution; **(b)** Cylindrical shell.

Free surface $\sum_1 = \sum_1\,(t)$ is the wetted surface of the rigid shell, and $\sum_0 = \sum_0\,(t)$ represents the free surface of the liquid, the shape and position of which depend on time.

Assume that in the equilibrium state at $t = 0$ we have $\sum_0(0) = S_0$, i $\sum_0\,(0) = S_1$. The reservoir is associated with a Cartesian coordinate system $0xyz$, the free surface of the liquid S_0 is located in the plane $z = 0$ in the state of rest. The surface $z = -H$ is the bottom of the shell. When an external excitation acts on the shell, the surfaces $\sum_0$ and $\sum_1$ change their shape over time. If a shell of revolution is considered, the surface S_0 is a circle of radius R, **Figure 1a**).

The problem of determining the oscillations is considered for an ideal (inviscid, incompressible) and irrotational fluid located in a rigid axisymmetric shell of revolution (e.g., cylindrical, conical, spherical, etc.), partially filled with the liquid. Since the shell is considered perfectly rigid, the motion of the fluid is considered relative to it. External loads are incorporated in terms of shell accelerations (or, equivalently, inertial forces in a non-inertial reference frame), namely the horizontal acceleration $a_x(t)$ along the x-axis, the vertical acceleration $a_z(t)$, and the gravitational acceleration g acting along the z-axis.

Consider the domain $Q(t)$, occupied by the liquid in the shell of revolution. In the cylindrical coordinate system, it can be defined as:

$$Q(t) = \{0 \le \theta \le 2\pi,\ \ 0 \le r \le r(z),\ -H \le z \le \zeta(r, \theta, t)\}\,.$$

Since the fluid in the shell is ideal and incompressible, and surface tension is neglected, the mass conservation law leads to the following continuity equation in the domain $Q(t)$:

$$\mathrm{div}\mathbf{V} = 0 \tag{1}$$

where $\mathbf{V}$ is the fluid velocity.

Let ρ be the fluid density, and the fluid is under the action of an external body force $\boldsymbol{F}_Q$ with acceleration $\boldsymbol{a}$, namely:

$$\boldsymbol{F}_Q = \iiint_{Q(t)} \rho \mathbf{a} dQ(t). \tag{2}$$

According to the momentum conservation law, the fluid motion is described as:

$$\rho \left(\frac{\partial \mathbf{V}}{\partial t} + (\mathbf{V} \cdot \nabla)\, \mathbf{V} \right) = -\nabla p + \mathbf{a}, \tag{3}$$

where p is the fluid pressure, and t is time.

Assume that the fluid motion is irrotational ($\mathrm{rot}\mathbf{V} = 0$). Then there exists a scalar velocity potential $\Phi = \Phi(x, y, z, t) = \Phi(\boldsymbol{r}, t)$, such that:

$$\mathbf{V} = \nabla\, \Phi. \tag{4}$$

From Equations (1)–(4), it follows that the velocity potential satisfies the Laplace equation in the time-varying fluid volume $Q(t)$:

$$\nabla^2 \Phi = 0. \tag{5}$$

Note that the acceleration $\mathbf{a}$ is expressed as follows:

$$\mathbf{a} = \mathbf{a}_x + \mathbf{a}_z + \mathbf{g},\ \ \mathbf{a}_x = -\nabla\left(x a_x(t)\right),\ \mathbf{a}_z = -\nabla\left(z a_z(t)\right),\ \mathbf{g} = -\nabla(zg).$$

That is,

$$\boldsymbol{a} = -\nabla\left(x a_x(t) + z a_z(t) + gz\right). \tag{6}$$

Thus, from Equations (3), (4), and (6), we have:

$$\frac{\partial \Phi}{\partial t} + \frac{1}{2}(\nabla\Phi, \nabla\Phi) + \frac{1}{\rho}p + xa_x(t) + z\left(g + a_z(t)\right) = C(t). \tag{7}$$

The function $C(t)$ on the right side of Equation (7) is neglected by incorporating it into the potential Φ. Thus, the Bernoulli equation is obtained in the form:

$$p - p_0 = -\rho\left[\frac{\partial \Phi}{\partial t} + xa_x(t) + \left(g + a_z(t)\right)z + \frac{1}{2}(\nabla\Phi, \nabla\Phi)\right], \tag{8}$$

where p_0 is atmospheric pressure. Thus, to find the fluid pressure, it is necessary to determine the potential φ from the Laplace equation.

We now proceed to the formulation of the boundary conditions for the Laplace Equation (5) in the domain $Q(t)$, bounded by the surfaces $\Sigma_0(t)$ and $\Sigma_1(t)$.

On the wetted surface of the shell $\Sigma_1(t)$ (rigid wall), the no-flow (no-penetration) condition is satisfied:

$$\left.\frac{\partial \Phi}{\partial \mathbf{n}}\right|_{\Sigma_1} = 0, \tag{9}$$

where $\mathbf{n}$ is the external unit normal to the wetted surface $\Sigma_1(t)$.

On the free surface $\Sigma_0(t)$ the kinematic and dynamic conditions must be satisfied. Let us consider the kinematic condition. This implies that a fluid particle remains on the free surface $\Sigma_0(t)$ throughout the motion, provided that it was located on this surface at the initial time. Let us assume that the free surface is represented in the form $G(x, y, z, t) = 0$. According to the formulated condition, the derivative of the function G must be equal to zero at any moment of time, namely:

$$\frac{dG}{dt} = \frac{\partial G}{\partial t} + (\mathbf{V}\cdot\nabla G) = \frac{\partial G}{\partial t} + (\nabla\Phi\cdot\nabla G) = 0.$$

Taking into account that $G(x, y, z, t) = z - \zeta(x, y, t) = 0$, we obtain the kinematic condition on the free surface in the form:

$$\frac{\partial \zeta}{\partial t} + \frac{\partial \zeta}{\partial x}\frac{\partial \Phi}{\partial x} + \frac{\partial \zeta}{\partial y}\frac{\partial \Phi}{\partial y} - \frac{\partial \Phi}{\partial z} = 0. \tag{10}$$

Since the unit outward normal to the surface $z = \zeta(x, y, t)$ has the form

$$\mathbf{n} = \left(-\frac{\partial \zeta}{\partial x}, -\frac{\partial \zeta}{\partial y}, 1\right)/\sqrt{1 + |\nabla\zeta|^2},$$

then the kinematic condition (10) is given in the following form:

$$\frac{\partial \Phi}{\partial \boldsymbol{n}} = \frac{\partial \zeta/\partial t}{\sqrt{1 + |\nabla\zeta|^2}}, \tag{11}$$

where the function $\zeta(x, y, t)$ describes the location and motion of the free surface $\Sigma_0(t)$ over time. This function is unknown in advance; for the formulation of the problem, we use the dynamic boundary condition on $\Sigma_0(t)$ as follows:

$$\frac{\partial \Phi}{\partial t} + xa_x(t) + \left(g + a_z(t)\right)\zeta + \frac{1}{2}(\nabla\Phi, \nabla\Phi) = 0. \tag{12}$$

Condition (12) means, according to (8), that the fluid pressure on the free surface is equal to the atmospheric pressure p_0.

Thus, the determination of the irrotational motion of an ideal incompressible fluid in rigid tanks leads to a nonlinear boundary-value problem with two unknown functions, namely, the shape of the free surface ζ and the fluid potential Φ. This problem is formulated:

$$\nabla^2\Phi = 0,\ \left.\frac{\partial\Phi}{\partial\mathbf{n}}\right|_{\Sigma_1} = 0,\ \frac{\partial\Phi}{\partial\mathbf{n}} = \left.\frac{\partial\zeta/\partial t}{\sqrt{1+|\nabla\zeta|^2}}\right|_{\Sigma_0}, \\ \frac{\partial\Phi}{\partial t} + xa_x(t) + (g+a_z(t))\,\zeta + \frac{1}{2}(\nabla\Phi\cdot\nabla\Phi) = 0\Big|_{\Sigma_0}. \tag{13}$$

The formulated Neumann problem (13) is supplemented by the solvability condition [26], representing the conservation of fluid volume:

$$\iiint_{Q(t)} dQ(t) = 0. \tag{14}$$

Equations (12)–(14) describe the liquid sloshing problem in a nonlinear formulation. The boundary value problem (12)–(14) must be solved with initial conditions to obtain a unique solution. It is usually assumed that the initial position of the free surface $\sigma_0(0)$ and the fluid potential φ are given in the form (corresponding to the state of rest):

$$\zeta(x,y,0) = \zeta_0(x,y) = 0, \qquad \left.\frac{\partial\Phi}{\partial\mathbf{n}}\right|_{S_0} = \varphi(x,y,0). \tag{15}$$

This is the complete nonlinear formulation of the problem within the potential theory with a moving free surface. For shells of revolution, the problem is solved in cylindrical or special curvilinear coordinates, taking into account the shape of the meridian. A direct solution of the nonlinear boundary value problem is challenging; therefore, the multimodal Lukovsky-Miles method (based on the Bateman-Luke variational principle or projection onto basis functions) is employed in this work. In doing so, we find the linear natural modes of fluid oscillations in a rigid shell (the solution of the linear problem), namely, the basis functions $\varphi_k(\rho,\theta,z)$ in the cylindrical coordinate system (ρ,θ,z) to determine the potential φ, the functions $f_k(r,\theta)$ for describing the free surface elevation ζ, as well as the natural frequencies ω_k (or $\chi_k = \omega_k^2/g$).

The basis functions $\varphi_k(\rho,\theta,z)$ satisfy the Laplace equation $\Delta\varphi_k = 0$ in the domain $Q(0)$ and the no-flow condition $\partial\varphi_k/\partial\mathbf{n} = 0$ on the rigid wall $\Sigma_1(0) = S_1$.

Next, we expand the solution of the nonlinear boundary value problem (13)–(15) into a series in terms of these modes:

$$\Phi(\rho,\theta,z,t) = \sum\nolimits_{k=1}^{\infty} \dot{q}_k(t)\,\varphi_k(r,\theta,z), \tag{16}$$

$$\zeta(\rho,\theta,t) = \sum\nolimits_{k=1}^{\infty} q_k(t)\,\zeta_k(r,\theta). \tag{17}$$

Here $q_k(t)$ are generalized coordinates.

In the subsequent subsections, the construction of these basis functions will be described. Let us introduce the action functional (the Bateman–Luke variational functional) as follows:

$$\mathcal{W}=\int_{t_1}^{t_2} L\,\mathrm{dt},\quad L=\iiint_{Q(t)}\left(\frac{\partial\Phi}{\partial t}+\frac{1}{2}\mid\nabla\Phi\mid^2+gz\right)dV, \tag{18}$$

or in an equivalent «pressure integral» form:

$$L=-\int_{Q(t)} p\,dV.$$

After substituting the expansions (16) and (17) into L and integrating over the volume $Q(t)$ (which itself depends on **q**) we obtain the ordinary Lagrangian $L(\mathbf{q},\dot{\mathbf{q}})$.

Next, we apply the Euler-Lagrange equations for each i:

$$\frac{d}{dt}\left(\frac{\partial L}{\partial \dot{q}_i}\right)-\frac{\partial L}{\partial q_i}=0,$$

and obtain a system of second-order nonlinear ordinary differential equations in the form:

$$\mathbf{M}\left(\mathbf{q}\right)\ddot{\mathbf{q}}+\mathbf{N}\left(\mathbf{q},\dot{\mathbf{q}}\right)+\mathbf{K}\left(\mathbf{q}\right)=\mathbf{F}(t), \tag{19}$$

where **M** is the mass matrix depending on the free-surface geometry, **N** is the vector of nonlinear quadratic and cubic terms associated with convective and free-surface effects, **K** is the nonlinear stiffness vector, and $\mathbf{F}(t)$ is the external forcing vector.

In the case of weak nonlinearity [11,37], Equation (19) takes the form:

$$\ddot{q}_i+\omega_i^2 q_i+\sum\nolimits_{j,k} A_{ijk}\,q_j q_k+\sum\nolimits_{j,k,l} B_{ijkl}\,q_j q_k q_l+\sum\nolimits_{j,k} D_{ijk}\,\dot{q}_j\dot{q}_k=f_i(t), \quad i=1,2,\ldots,N, \tag{20}$$

where ω_i are natural frequencies of linear modes,

A_{ijk} are quadratic coefficients (usually small or absent due to symmetry in antisymmetric modes),

B_{ijkl} is cubic coefficients (the most significant for resonance),

D_{ijk} is coefficients at $\dot{q}_j\dot{q}_k$ (at the convective terms $\mid\nabla\Phi\mid^2$),

$f_i(t)$ is the forcing force, which is proportional to the tank's acceleration. That is, using the Lukovsky–Miles multimodal approach [11, 12, 37], the initial nonlinear boundary value problem (13)–(15) is reduced to solving a finite nonlinear system of ordinary differential equations suitable for analysing the dynamics of fluid-filled tanks under combined horizontal and vertical loads. For a specific shell shape (cylinder, cone, sphere), the basis functions can be obtained in the form of analytical expressions or by using numerical methods.

3. Construction of basis functions from the linear spectral boundary value problem

Let us formulate the problem of the free oscillations of a fluid in a rigid tank in a linear approximation. The fluid is considered ideal and incompressible, and its flow is assumed to be irrotational. At the same time, we assume that the surfaces $\Sigma_0(t),\ \Sigma_1(t)$ do not change with time; that is, the boundary conditions for the Laplace equation are considered on the surfaces S_0 and S_1, which correspond to the initial time, namely $S_0 = \Sigma_0(0)$, $S_1 = \Sigma_1(0)$:

$$\nabla^2\Phi = 0, \quad \left.\frac{\partial\Phi}{\partial\mathbf{n}}\right|_{S_1} = 0, \quad \left.\frac{\partial\Phi}{\partial\mathbf{n}}\right|_{S_0} = \frac{\partial\zeta}{\partial t}, \quad p - p_0|_{S_0} = 0. \tag{21}$$

To solve the boundary value problem (21), the mode superposition method is used, which is widely applied to solve coupled boundary value problems of dynamics [37], in particular, problems of fluid-structure interaction [38]. Its efficiency is due to the transition to generalized coordinates, which allows for a significant reduction in computational costs. Within the normal mode approach, the unknown functions Φ and ζ for shells of revolution are represented as expansions in terms of natural modes:

$$\Phi(x, y, z, t) = \sum\nolimits_{k=1}^{n} \dot{d}_k(t)\, \varphi_k(x, y, z), \tag{22}$$

$$\zeta(x, y, t) = \sum\nolimits_{k=1}^{n} d_k(t)\, \zeta_k(x, y), \tag{23}$$

where $\varphi_k(x, y, z)$ and $\zeta_k(x, y)$ are basis functions, $d_k(t)$ and $\dot{d}_k(t)$ are generalized coordinates and their time derivatives. The functions φ_k and ζ_k satisfy the following spectral boundary value problems [33]:

$$\nabla^2\varphi_k = 0, \quad \left.\frac{\partial\varphi_k}{\partial\mathbf{n}} = 0\right|_{S_1}, \quad \left.\frac{\partial\varphi_k}{\partial\mathbf{n}} = \frac{\chi_k^2}{g}\varphi_k\right|_{S_1}, \tag{24}$$

where χ_k is the natural frequency corresponding to the natural mode φ_k. Assume that the position of the free surface at the initial moment of time corresponds to the level $z = 0$. Then, according to (24), the free surface elevation $\zeta(x, y, t)$ can be expressed as:

$$\zeta(x, y, t) = \frac{1}{g}\sum\nolimits_{k=1}^{n} \chi_k^2 d_k(t)\varphi_k(x, y, 0). \tag{25}$$

Thus, the basis functions for evaluating both φ and ζ can be determined using the functions $\varphi_k(x, y, z)$. It should be noted that the boundary value problem (24) is a spectral boundary value problem [36]. Its solution yields a system of basis functions, which is subsequently used to model fluid motion in tanks, in both linear and nonlinear formulations, under the action of external disturbing forces.

4. System of singular integral equations and 2π-periodicity of integral operators

A set of basis functions $\{\varphi_k(x,\ y,\ z)\}$, used for approximating fluid sloshing modes in shells of revolution, is determined by solving a system of singular integral equations. The specified system is formulated within the conceptual approach proposed in Lukovsky [39] and Brebbia et al. [40]. Simplify the notation; we hereafter omit the index k; then the main integral relation, which defines the function $\varphi_k(x, y, z)$, can be written as follows:

$$2\pi\varphi(\mathbf{r}_0) = \iint_{\sigma} q(\mathbf{r}) \frac{1}{|\mathbf{r} - \mathbf{r}_0|} d\sigma - \iint_{\sigma} \varphi(\mathbf{r}) \frac{\partial}{\partial \mathbf{n}} \frac{1}{|\mathbf{r} - \mathbf{r}_0|} d\sigma, \quad \sigma = S_1 \cup S_0, \tag{26}$$

where $\mathbf{r} = (x, y, z)$, $\mathbf{r}_0 = (x_0, y_0, z_0)$ are points on the boundary surface σ, $|\mathbf{r} - \mathbf{r}_0|$ is the Cartesian distance between the points $\mathbf{r}$ and $\mathbf{r}_0$, $q(\mathbf{r})$ is the normal derivative of the function $\varphi(\mathbf{r})$ on the surface σ.

For a surface of revolution, the domain Ω, occupied by the fluid, is a body of revolution, and to solve the boundary-value problems (24), it is advisable to use a cylindrical coordinate system (ρ, θ, z), where,

$$x = \rho\cos\theta, \quad y = \rho\sin\theta, \quad \mathrm{z} = \mathrm{z},$$

$$|\mathbf{r} - \mathbf{r}_0| = \sqrt{\rho^2 + \rho_0^2 - 2\rho\rho_0\cos(\theta - \theta_0) + (z - z_0)^2}.$$

Consider the following integral operator:

$$(G\gamma)(\mathbf{r_0}) = \iint_{\sigma} \gamma(\mathbf{r}) G(|\mathbf{r} - \mathbf{r}_0|)\, d\sigma, \tag{27}$$

whose kernel depends only on the distance $|\mathbf{r} - \mathbf{r}_0|$. Suppose that,

$$\gamma(\mathbf{r}) = f(\rho, z)\cos(l\theta). \tag{28}$$

If Γ is the surface generatrix σ, then, representing the double integral in (27) as an iterated integral at the point $\mathbf{r}_0 = (\rho_0, \theta_0, z_0)$, we obtain:

$$(G\gamma)(\mathbf{r_0}) = \int_{\Gamma} f(\rho, z)\{\int_0^{2\pi} \cos(l\theta)\, G(|\mathbf{r} - \mathbf{r}_0|)\, d\theta\}\mathrm{d}\Gamma. \tag{29}$$

In the inner integral in (29), we make a change of variable: $\psi = \theta - \theta_0, \theta = \psi + \theta_0$. As a result of the trigonometric identity:

$$\cos\ (l(\psi + \theta_0)) = \cos(l\psi)\cos(l\theta_0) - \sin(l\psi)\sin(l\theta_0),$$

and 2π- periodicity of the functions in the inner integral in (29), we obtain:

$$\int_0^{2\pi} \sin(l\theta)G(|\,\mathbf{r} - \mathbf{r}_0\,|)\, d\theta = \int_{-\pi}^{\pi} \sin(l\theta)G(|\,\mathbf{r} - \mathbf{r}_0\,|)\, d\theta = 0,$$

$$\int_0^{2\pi} \cos(l\theta)G(|\,\mathbf{r} - \mathbf{r}_0\,|)\, d\theta = \cos(l\theta_0) \int_0^{2\pi} \cos(l\psi)G(|\,\mathbf{r} - \mathbf{r}_0\,|)\, d\psi.$$

So,

$$(G\gamma)(\mathbf{r}_0) = f_1(\rho_0, z_0)\cos(l\theta_0),$$

where $f_1(\rho_0, z_0) = \int_\Gamma f(\rho, z)\{\int_0^{2\pi} \cos(l\psi)\, G(|\mathbf{r} - \mathbf{r}_0|)\, d\psi\}\mathrm{d}\Gamma$.

Thus, the integral operators in (26) are 2π is periodical, This allows for the expansion of unknown functions into Fourier series:

$$\Phi(\rho,\theta,z,t)=\sum\nolimits_{k=1}^{n}\sum\nolimits_{l=0}^{m}\dot{d}_{kl}(t)\,\varphi_{kl}(\rho,z)\cos(l\theta), \tag{30}$$

$$\zeta(\rho,\theta,t)=\sum\nolimits_{k=1}^{n}\sum\nolimits_{l=0}^{m}d_{kl}(t)\,\zeta_{kl}(\rho)\cos(l\theta), \tag{31}$$

The use of expansions (30) and (31) allows for reducing the problem of determining the basis functions $\varphi_k(x,y,z)$ to solving a one-dimensional system of singular integral equations.

5. Analysis of kernel properties and numerical solution of singular integral equation systems

Taking into account expansions (30) and (31), we reduce the boundary value problem (21) to a system of one-dimensional singular integral equations in the form [33]:

$$\begin{gathered}2\pi\varphi(\rho(z_0),z_0)+\int_\Gamma\varphi(\rho(z),z)\,\Theta(z,z_0)\,\rho(z)\,d\Gamma-\\ \chi^2\int_0^{R_0}\varphi(\rho,0)\,\Phi(\mathbf{r},\mathbf{r}_0)\,\rho\,d\rho=0,\quad \mathbf{r}_0\in S_1,\\ 2\pi\varphi(\rho,0)+\int_\Gamma\varphi(\rho(z),H)\,\Theta(z,z_0)\,\rho(z)\,d\Gamma-\\ \chi^2\int_0^{R_0}\varphi(\rho,H)\,\Phi(\mathbf{r},\mathbf{r}_0)\,\rho\,d\rho=0,\quad \mathbf{r}_0\in S_0,\end{gathered} \tag{32}$$

where R_0 is the radius of the free surface,

$$\Theta(z,z_0)=\frac{4}{\sqrt{a+b}}\left\{\frac{1}{2r}\left[\frac{r^2-r_0^2+(z_0-z)^2}{a-b}E_l(k)-F_l(k)\right]n_r+\frac{z_0-z}{a-b}E_l(k)n_z\right\},$$

$$\Phi(\mathbf{r},\mathbf{r}_0)=\frac{4}{\sqrt{a+b}}F_l(k),\quad a=\rho^2+(z-z_0)^2,\quad b=2\rho r_0.$$

$$E_l(k)=(-1)^l(1-4l^2)\int_0^{\pi/2}\cos(2l\theta)\sqrt{1-k^2\sin^2\theta}\,d\theta,$$

$$F_l(k)=(-1)^l\int_0^{\pi/2}\frac{\cos(2l\theta)}{\sqrt{1-k^2\sin^2\theta}}\,d\theta,\quad k^2=\frac{2b}{a+b}.$$

For the values of k, approaching 1, there is an asymptotic expansion for the function $F_0(k)$,

$$\begin{gathered}F_0(k)=\ln\frac{4}{k'}+\left(\frac{1}{2}\right)^2\left(\ln\frac{4}{k'}-\frac{2}{1\cdot 2}\right)k'^2+\\ \left(\frac{1\cdot 3}{2\cdot 4}\right)^2\left(\ln\frac{4}{k'}-\frac{2}{1\cdot 2}-\frac{2}{3\cdot 4}\right)k'^4+...,\ k'^2=1-k^2,\end{gathered} \tag{33}$$

from which the logarithmic singularity of the kernel $\Phi\left(\mathbf{r},\mathbf{r}_0\right)$ follows. Next, we consider the kernel $\Theta\left(z,z_0\right)$. We introduce the function:

$$Q\left(z,z_0\right)=\frac{n_r}{2r}\frac{r_0^2-r^2+(z_0-z)^2}{a-b}+\frac{z_0-z}{a-b}n_z,$$

which is the coefficient of the function $E_l(k)$ in the kernel $\Theta(z, z_0)$. It is proven below that $Q(z, z_0)$ is bounded at $z \to z_0$.

Since the singular domain under consideration is small, the following approximate equalities, obtained from Taylor series expansions, hold:

$$a - b = (r - r_0)^2 + (z - z_0)^2 \approx (1 + (r_0^{'})^2)(z - z_0)^2.$$

Then,

$$Q(z, z_0) \approx \frac{1}{(z_0 - z)(1 + (r_0^{'})^2)} \left[\frac{n_r(2r_0 r_0^{'} + (z_0 - z))}{2r_0} + n_z \right].$$

According to the definition of the non-unit normal to the surface $\mathbf{n}_1$, we obtain:

$$\mathbf{n}_1 = \begin{vmatrix} \mathbf{i} & \mathbf{j} & \mathbf{k} \\ -r\sin\theta & r\cos\theta & 0 \\ r^{'}\cos\theta & r^{'}\sin\theta & 1 \end{vmatrix} = \mathbf{i}r\cos\theta + \mathbf{j}r\sin\theta + \mathbf{k}\left(-r^{'}r\right),$$

Then,

$$\mid \mathbf{n}_1 \mid^2 = r^2 + r^2(r^{'})^2 = r^2(1 + (r^{'})^2),$$

and for the unit normal, we have:

$$n_r = \frac{1}{\sqrt{1 + (r^{'})^2}}, n_z = \frac{-r^{'}}{\sqrt{1 + (r^{'})^2}}.$$

Then, $n_r r_0^{'} + n_z = 0$. Thus as $z \to z_0$ we obtain:

$$Q\left(z, z_0\right) \to \frac{n_r}{2r_0(1 + (r_0^{'})^2)} = \frac{1}{2r_0\left(\sqrt{1 + (r_0^{'})^2}\right)^3}.$$

So the function $Q(z, z_0)$ remains bounded as $z \to z_0$. Therefore, the kernel $\Theta(z, z_0)$ also has a logarithmic singularity.

We will use special quadrature formulas for computing integrals with a logarithmic weight, based on the analytical formula

$$\int_0^1 x^n \ln\frac{1}{x} dx = \frac{1}{(n+1)^2}.$$

We construct orthogonal polynomials $\{P_n(x)\}_{x=0}^{n}$with the logarithmic weight function as follows:

$$\int\limits_0^1 P_i(x)P_k(x)\ln\frac{1}{x}dx = \begin{cases} \|P_i(x)\|^2, & i = k \\ 0, & i \neq k \end{cases}$$

Introduce the determinant:

$$P_n(x) = \begin{vmatrix} \left(\frac{1}{2}\right)^2 & \left(\frac{1}{3}\right)^2 & \cdots & \left(\frac{1}{n}\right)^2 & \left(\frac{1}{n+1}\right)^2 & \\ \left(\frac{1}{2}\right)^2 & \left(\frac{1}{3}\right)^2 & \left(\frac{1}{4}\right)^2 & \cdots & \left(\frac{1}{n+1}\right)^2 & \left(\frac{1}{n+2}\right)^2 \\ \left(\frac{1}{3}\right)^2 & \left(\frac{1}{4}\right)^2 & \left(\frac{1}{5}\right)^2 & \cdots & \left(\frac{1}{n+2}\right)^2 & \left(\frac{1}{n+3}\right)^2 \\ \vdots & \vdots & \vdots & \ddots & \vdots & \vdots \\ \left(\frac{1}{n}\right)^2 & \left(\frac{1}{n+1}\right)^2 & \left(\frac{1}{n+2}\right)^2 & \cdots & \left(\frac{1}{2n-1}\right)^2 & \left(\frac{1}{2n}\right)^2 \\ 1 & x & x^2 & \cdots & x^{n-1} & x^n \end{vmatrix}$$

For the first polynomials, we have the expressions

$$\begin{cases} P_0(x) = 1 \\ P_1(x) = \begin{vmatrix} 1 & \left(\frac{1}{2}\right)^2 \\ 1 & x \end{vmatrix} = x - \frac{1}{4} \\ P_2(x) = \begin{vmatrix} 1 & \left(\frac{1}{2}\right)^2 & \left(\frac{1}{3}\right)^2 \\ \left(\frac{1}{2}\right)^2 & \left(\frac{1}{3}\right)^2 & \left(\frac{1}{4}\right)^2 \\ 1 & x & x^2 \end{vmatrix} = \frac{7}{144}x^2 - \frac{5}{144}x + \frac{17}{5184} \end{cases}$$

Table 1 presents the weighting coefficients and roots of the obtained polynomials, which allows for the construction of efficient quadrature formulas for calculating integrals with logarithmic singularities [37].

Table 1. Weights and roots of orthogonal polynomials with a logarithmic weight.

n	w_i (weighting coefficients)	x_i (roots of polynomials)
2	0.71853931	0.11200880
	0.28146068	0.60227691
3	0.51340455	0.063890792
	0.39198004	0.36899706
	0.094615406	0.76688030
4	0.38346406	0.041448480
	0.38687532	0.24527491
	0.19043513	0.55616545
	0.039225487	0.84898239
5	0.29789346	0.029134472
	0.34977622	0.17397721
	0.23448829	0.41170251
	0.098930460	0.67731417
	0.018911552	0.89477136
6	0.23876366	0.021634005
	0.30828657	0.12958339
	0.24531742	0.31402045
	0.14200875	0.53865721
	0.055454622	0.75691533
	0.010168958	0.92266884

Methods developed in Karaiev and Strelnikova [41] and Strelnikova et al. [42] are used for the numerical solution of the system of singular integral equations (Equation (32)).

6. System of differential equations for the linear boundary-value problem with Rayleigh damping

As a result of solving the spectral boundary-value problem (24) using the integral representation (26) and the boundary super-element method, the natural frequencies χ_{kl} and the corresponding mode shapes φ_{kl} of liquid oscillations in a rigid tank have been determined, $k = \overline{1,n}$, $l = \overline{0,m}$. Consequently, the expansions (22) and (23) can be employed to approximate the unknown functions—the velocity potential φ and the free-surface elevation ζ.

For the analysis of liquid motion in axisymmetric shells, the pressure p is defined as follows [12]:

$$\frac{p}{\rho_l} = -\frac{\partial \Phi}{\partial t} - (g + a_v(t))z + a_h(t)x + \frac{p_0}{\rho_l}, \tag{34}$$

where g, $a_h(t)$, and $a_v(t)$ denote the gravitational acceleration and the horizontal and vertical excitation accelerations, respectively, and $_l$ is the liquid density.

From Equation (34), a nonhomogeneous system of second-order Mathieu-type ordinary differential equations is derived [43]:

$$\begin{gathered}
\ddot{d}_{k0}(t) + 2\omega_{k0}\xi\,\dot{d}_{k0}(t) + \omega_{k0}^2\left(1 + \frac{a_v(t)}{g}\right) d_{k0}(t) = 0, \\
\ddot{d}_{k1}(t) + 2\omega_{k1}\xi\,\dot{d}_{k1}(t) + \omega_{k1}^2\left(1 + \frac{a_v(t)}{g}\right) d_{k1}(t) + a_h(t)F_{k1} = 0, \\
F_{k1} = \frac{(r,\varphi_{k1})}{(\varphi_{k1},\varphi_{k1})}, \ddot{d}_{kl}(t) + 2\omega_{kl}\xi\,\dot{d}_{kl}(t) + \omega_{kl}^2\left(1 + \frac{a_v(t)}{g}\right) d_{kl}(t) = 0, \\
k = \overline{1,n},\ l = \overline{2,m}.
\end{gathered} \tag{35}$$

System (35) is supplemented with the initial conditions:

$$d_{kl}(0) = d_{kl}^0,\ \ \dot{d}_{kl}(0) = d_{kl}^1,\ \ k = \overline{1,n},\ \ l = \overline{0,m}. \tag{36}$$

The system of differential equations (35), together with the initial conditions (36), describes the dynamic response of the liquid in the shell under combined vertical and horizontal excitations. The governing equations are formulated in terms of the modal coordinates $d_{kl}(t)$, which characterize the oscillations of the free surface.

To account for minimal dissipative effects, artificial viscous damping proportional to velocity, $2\omega_{kl}\xi\dot{d}_{kl}(t)$, is introduced into the originally undamped formulation, where ξ is the damping ratio [1].

It should be noted that, within the framework of the linear approach, the amplitude theoretically tends to infinity at resonance. However, under real conditions, even at small amplitudes, energy dissipation occurs due to a number of physical mechanisms. The main contributors are viscous boundary layers near the tank walls and bottom, the generation of weak vorticity, surface effects, contamination of the free surface, minor wave breaking, and surface tension effects.

To account for these dissipative effects in linear modal theory, artificial damping is introduced. One of the most widely used approaches is the Rayleigh damping model (also known as proportional damping).

In this model, we employ the equations given above (Equation (35)). In the subsequent analysis, Rayleigh damping in the ideal fluid model is applied with a damping ratio ξ ranging from 0.005 to 0.05, which corresponds to the values reported for viscous fluid damping in liquid sloshing [44] and typical stabilization practices in FSI sloshing simulations [45,46].

7. Governing system of differential equations for the nonlinear problem in generalized coordinates

Following Brebbia et al. [40], the unknown functions describing the velocity potential and the free-surface elevation are represented in the form:

$$\begin{aligned} \Phi(r,z,\theta,t) &= \dot{q}_{11}(t)\Phi_{11}(r,z)\cos\theta + \dot{q}_{01}(t)\Phi_{01}(r,z) + \dot{q}_{21}(t)\Phi_{21}(r,z)\cos 2\theta, \\ \zeta(r,z,\theta,t) &= \mathrm{q}_{11}(t)\zeta_{11}(r,z)\cos\theta + \mathrm{q}_{01}(t)\zeta_{01}(r,z) + \mathrm{q}_{21}(t)\zeta_{21}(r,z)\cos 2\theta, \end{aligned} \tag{37}$$

where the basis functions $\Phi_{kl}(r,z)$ and $\zeta_{kl}(r,z)$ are obtained from the solution of the linear spectral boundary-value problem (24).

It is assumed that the horizontal excitation acts strictly in a single direction (along the Ox axis only, with no Oy component), the initial conditions are zero, and the oscillation amplitude remains moderate, i.e., $\zeta_{\text{max}}/R \lesssim 0.15$–$0.25$.

By employing the nonlinear boundary conditions (13), the following reduced system of nonlinear second-order ordinary differential equations is derived in Lukovsky et al. [47]:

$$\begin{aligned} \ddot{q}_{11} + \chi_{11}^2\left(1+\frac{a_z(t)}{g}\right)q_{11} + \alpha_1 q_{11}^3 + \alpha_2 q_{11}\dot{q}_{11}^2 + \beta q_{01}q_{11} + \gamma q_{21}q_{11} &= a_x(t), \\ \ddot{q}_{01} + \chi_{01}^2 q_{01}\left(1+\frac{a_z(t)}{g}\right) + \delta\left(q_{11}\ddot{q}_{11} + \dot{q}_{11}^2\right) &= 0, \\ \ddot{q}_{21} + \chi_{21}^2 q_{21}\left(1+\frac{z(t)}{g}\right) + \varepsilon\left(q_{11}\ddot{q}_{11} - \dot{q}_{11}^2\right) &= 0, \end{aligned} \tag{38}$$

where small higher-order cubic terms are neglected.

Next, the asymptotic principle of Narimanov-Moiseev [48] is applied, i.e., the concept of asymptotic slaving of secondary modes. Within this framework, the secondary modes—the axisymmetric mode $q_{01}$and the second harmonic mode q_{21}—are expressed in terms of the square of the primary mode amplitude using the approximation:

$$q_{01} \approx c\, q_{11}^2, \quad q_{21} \approx d\, q_{11}^2. \tag{39}$$

The coefficients c and d are derived by applying the Narimanov–Moiseev asymptotic procedure to the infinite-dimensional nonlinear modal system obtained via the Lukovsky–Miles variational formulation. Since the natural frequencies of the secondary modes are far from resonance, their inertial terms can be neglected at the leading order. This reduces the equations for q_{01} and q_{21} to algebraic relations.

The hydrodynamic integrals are then computed from the following formulas:

$$I_{m,n}^{(p,q)} = \iint_{S_0} \Phi_{mn}\Phi_{pq}^2 \, dS, \quad J_{m,n}^{(p,q)} = \iint_{S_0} \Phi_{mn}\Phi_{pq}^3 \, dS. \tag{40}$$

For a cylindrical tank, the basis functions are separable, which significantly simplifies the computation of the hydrodynamic coefficients. The integrals $I_{m,n}^{(p,q)}$ and $J_{m,n}^{(p,q)}$reduce to ordinary one-dimensional integrals over the vertical coordinate, which can be evaluated with high accuracy both analytically and numerically:

$$I_{m,n}^{(p,q)} = \int_0^H \psi_{mn}(z) \left[\psi_{pq}(z)\right]^2 dz, \;\; J_{m,n}^{(p,q)} = \int_0^h \psi_{mn}(z) \left[\psi_{p,q}(z)\right]^3 dz, \tag{41}$$

where $\psi_{mn}(z)$ are the normalized vertical basis functions.

In the case of arbitrary shells of revolution, the basis functions are non-separable in the cylindrical coordinates (r, z). So, the shell geometry is described parametrically using the arc-length coordinate $s$along the meridian, where $r = r(s)$ and $z = z(s)$. The linear natural sloshing modes $\Phi_{mn}(s)$ are determined numerically, typically by the boundary element method. The hydrodynamic integrals $I_{m,n}^{(p,q)}$ and $J_{m,n}^{(p,q)}$are then computed by direct numerical integration along the meridian, taking into account the surface element $dS = 2\pi r(s)\, ds$.

Then the hydrodynamic coefficients $d_{i1}^{(2)}$, α_{mn}, β_m, and γ_m are expressed through the hydrodynamic integrals as in Lukovsky et al. [47].

After evaluating the required integrals, the slaving (intermodal) coefficients are obtained as:

$$c = -\frac{d_{01}^{(2)}}{2\alpha_{01}\chi_{01}^2}, d = -\frac{d_{21}^{(2)}}{\alpha_{2,1}\chi_{21}^2}. \tag{42}$$

Substitution of these asymptotic relations into system (38) yields an effective nonlinear equation governing the primary modal coordinate $q_{11}(t)$:

$$\ddot{q}_{11} + \chi_{11}^2 \left(1 + \frac{a_z(t)}{g}\right) q_{11} + K_3 q_{11}^3 + K_4 q_{11}\dot{q}_{11}^2 = a_x(t), \tag{43}$$

where $q_{11}(t)$ is the generalized coordinate associated with the fundamental mode ($l = 1, n = 1$), χ_{11} is its natural frequency, and the coefficients K_3 and K_4 arise from both the direct cubic nonlinearities and the contributions of the asymptotically enslaved secondary modes. These effective nonlinear coefficients in the reduced modal equation are formed as follows:

$$K_3 = \alpha_3 + \beta_3\, c + \gamma_3\, d, \quad K_4 = \alpha_4 + \beta_4\, c + \gamma_4\, d, \tag{44}$$

where K_3 is the cubic stiffness coefficient (Duffing-type term), K_4 is the convective (velocity-dependent) nonlinear coefficient, α_3, α_4 represent direct contributions from the primary mode, β_3, β_4 represent contributions from the axisymmetric mode.

Table 2 below shows the variation of c, d, K_3, and K_4 across the range of aspect ratios ($0.3 \leq h/R \leq 2.0$). All coefficients in the present study were computed using the same consistent procedure according to Brebbia et al. [40], implemented in our in-house code.

Table 2. Values of slaving coefficients and effective nonlinear coefficients for different aspect ratios H/R .

h/R	c	d	K_3	K_4
0.30	−0.4812	0.2634	−1.928	0.682
0.50	−0.4127	0.2378	−1.704	0.631
0.70	−0.3679	0.2215	−1.521	0.592
1.00	−0.3468	0.2146	−1.452	0.554
1.50	−0.3305	0.2087	−1.379	0.521
2.00	−0.3241	0.2063	−1.347	0.507

Thus, the nonlinear dynamics of liquid sloshing in a cylindrical tank can be described by a single effective nonlinear differential equation for the dominant modal coordinate $q_{11}(t)$, derived within a third-order asymptotic multimodal framework [40], in which the secondary modes are expressed as quadratic functions of the primary mode amplitude according to relations (39).

In the present study, considering the dominance of the primary antisymmetric mode and applying the asymptotic slaving relations for the secondary modes, the free surface elevation can be approximated as:

$$\zeta(r,\theta,t) \approx q_{11}(t)\,\Phi_{11}(r,H)\cos\theta + c\,q_{11}^2(t)\,\Phi_{01}(r,H) + d\,\Phi_{11}(r,H)_1^2(t)\ \cos 2\theta,$$

where the first term represents the contribution of the primary antisymmetric mode ($m=1, n=1$), the second and third terms account for the quadratic contributions from the axisymmetric mode ($m=0, n=1$) and the $m=2$ mode, respectively, c and d are the slaving coefficients obtained from the asymptotic procedure and presented in **Table 2**. The maximum wave height at the wall ($r=R, \theta=0$) is then approximately:

$$\zeta_{\text{max}}(t) \approx q_{11}(t) + (c+d)q_{11}^2(t). \tag{45}$$

This quadratic correction plays an essential role in capturing the amplitude-dependent characteristics of the sloshing response.

8. Comparative analysis of Rayleigh-damped linear and nonlinear multimodal models

Although Rayleigh damping is widely used to stabilize linear potential flow models, its physical consistency and accuracy at large amplitudes remain questionable. In this section, the results obtained from the damped linear model are systematically compared with the nonlinear multimodal solution to highlight the regimes where the linear approximation remains acceptable and where nonlinear effects become dominant.

Consider the oscillations of a liquid in a rigid cylindrical tank. It is assumed that the tank of radius R is filled with an ideal incompressible liquid up to a height H (**Figure 1b**).

For $H = R = 1$ m, the natural frequencies and corresponding mode shapes of liquid oscillations in the tank are determined. The natural frequencies and the corresponding mode shapes of the liquid oscillations were determined by solving the linear eigenvalue problem. Convergence analysis showed that using the first three terms of the series expansion is sufficient. The obtained frequency values are given in **Table 3**.

Table 3. Natural frequencies of liquid oscillations in a rigid cylindrical tank, χ_{lk}^2/g.

l	Method	*k* = 1	*k* = 2	*k* = 3	*k* = 4	*k* = 5
0	BEM	3.828	7.017	10.177	13.327	16.476
	Ibrahim [1]	3.828	7.017	10.173	13.324	16.471
1	BEM	1.750	5.3320	8.538	11.707	14.866
	Ibrahim [1]	1.750	5.3319	8.536	11.706	14.863

Table 3 presents a comparison between the results obtained using the proposed BEM and the analytical data reported in Ibrahim [1]. The results demonstrate good agreement between the numerical and analytical solutions.

Figure 2 illustrates the mode shapes of the liquid-free-surface oscillations for $l = 0, 1$ and $k = 1, 2, 3$.

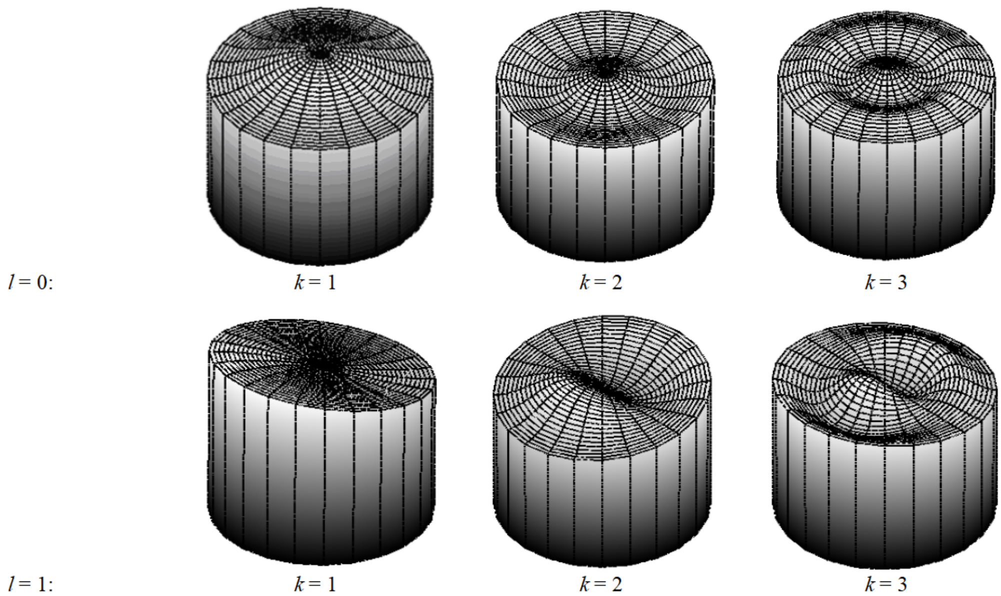

Figure 2. Free-surface oscillation modes in a rigid cylindrical tank.

Along the generator of the shell surface and the radius of the free surface, the following numbers of elements were used: $N_G = 260$ and $N_0 = 130$, respectively.

Next, forced oscillations of the liquid in the tank are considered within linear and nonlinear formulations, as well as forced oscillations with damping effects. The excitation is assumed in the form:

$$a_x(t) = A_x \cos(\omega_x t), \quad a_z(t) = A_z \cos(\omega_z t). \tag{46}$$

To assess the sensitivity of the sloshing response to the liquid filling depth, numerical simulations were performed for five different aspect ratios, **Table 4**.

Table 4. Effect of the aspect ratio h/R on the maximum wave elevation at the tank wall (planar motion).

h/R	χ_{11}(rad/s)	c	d	K_3	ζ_{max}/R
0.50	3.623	−0.4127	0.2378	−1.704	0.387
0.70	3.912	−0.3679	0.2215	−1.521	0.341
1.00	4.144	−0.3468	0.2146	−1.452	0.312
1.30	4.289	−0.3352	0.2114	−1.401	0.289
1.50	4.367	−0.3305	0.2087	−1.379	0.274

As demonstrated in **Table 4**, the maximum nondimensional wave elevation ζ_{max}/R increases significantly with decreasing h/R. This behavior is physically consistent with the strengthening of nonlinear modal interactions in shallower liquid. The obtained results provide useful guidance for engineering applications, indicating that tanks with lower filling ratios are more prone to large-amplitude sloshing under resonant vertical excitation.

To illustrate the influence of the liquid filling depth on the temporal evolution of sloshing, time histories of the wave elevation at the tank wall ($r = R$, $\theta = 0$) are presented in **Figure 3** for the aspect ratios: $H/R = 0.5$ (blue line), and 1.5 (black line). All simulations were performed under the same combined excitation conditions ($A_z = 0.0$, $\omega_x = \chi_{11}$, $A_x/g = 0.051$).

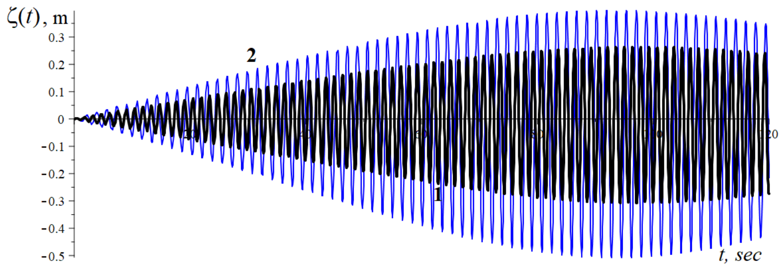

Figure 3. Time history of free-surface elevation at different H/R.

The results clearly demonstrate that shallower liquid depths lead to faster growth of the wave amplitude, which is consistent with the increase in the magnitude of the coefficient $|K_3|$. For the case $H/R = 1.0$, the response reaches a bounded steady state with $\eta_{max}/R \approx 0.30$, while at $H/R = 0.5$ the maximum elevation is noticeably larger due to stronger nonlinear modal interactions.

Having analyzed the influence of the filling ratio h/R on the nonlinear sloshing response, the study now proceeds to a comprehensive validation of the developed multimodal model. In the following section, the numerical results are compared with both the damped linear model and available data from the literature under various excitation conditions, including pure horizontal, pure parametric, and combined loading.

The maximum wave elevation obtained in the present nonlinear multimodal model is compared with available data in **Table 5**. For pure horizontal resonant excitation ($A_x/g = 0.051$), the computed maximum wave elevation reaches $\zeta_{max}/R \approx 0.274$–$0.387$, which agrees well with the classical results of Faltinsen and Timokha [7] and Liang et al. [46]. When an additional resonant vertical excitation is applied

($A_z/g = 0.102$), the wave elevation increases to 0.30–0.31. This moderate amplification due to combined loading is consistent with recent studies on combined excitations [47]. Higher values reported in the literature (up to 0.45–0.50R) are usually associated with stronger excitation amplitudes and the development of swirling motion. The present results therefore lie within the expected physical range and demonstrate the capability of the nonlinear model to capture the additional effect of parametric resonance.

Table 5. Comparison of the maximum nondimensional wave elevation $\zeta_{\max}/R$ at the tank wall under resonant or near-resonant excitation (*H/R* $\approx$ 1.0).

Source	Excitation type	Excitation parameters	ω_z/χ_{11}	ω_x/χ_{11}	$\zeta_{\max}/R$
Present study	Horizontal only	$A_x/g = 0.051$	–	1.00	0.274–0.387
Present study	Combined (horizontal + vertical)	$A_z/g = 0.102,\ A_x/g = 0.051$	1.00	1.00	0.30–0.31
Liang et al. [49]	Horizontal near resonance	$A_x/g \approx 0.05$–0.08	–	0.95–1.05	0.35–0.42
Faltinsen and Timokha [7]	Horizontal resonant (various cases)	$A_x/g \approx 0.02$–0.08	–	≈ 1.0	0.25–0.40
Lui et al. [50]	Combined (horizontal + vertical)	$A_x/g \approx 0.02$–$0.1,\ A_z/g \approx 0.02$–0.1	0.95–1.05	0.95–1.05	0.28–0.48

For the numerical analysis, the values of the loading parameters (45) presented in **Table 6** are adopted.

Table 6. Loading parameters.

Cases	A_x/g	A_z/g	ω_x	ω_z
A	0.051	0.0	4.144	-
B	0.051	0.102	1.0	8.288
C	0.051	0.102	4.144	4.144
D	0.5	1.0	3.0	7.1433

Case A represents pure horizontal resonance, Case B corresponds to parametric resonance, when the frequency of vertical excitation equals twice the first natural frequency for the first wave number. Case C corresponds to resonance phenomena caused by the coincidence of the sum of the excitation frequencies with twice the first natural sloshing frequency, whereas Case D represents subharmonic resonance, when the difference between the excitation frequencies equals the first fundamental frequency.

In **Figures 4–11**, curves labelled as 1 (black) describe the free-surface elevation obtained within the linear formulation without damping at the point $R = 1$, $\theta = 0$ on the free surface. Curves 2 (blue) in **Figures 4–7** correspond to the solution of the nonlinear Equation (43), where the coefficients K_3 and K_4 are (see **Table 2**),

$$K_3 = -1.452 \text{ and } K_4 = 0.554 \text{ at } H/R = 1.0,$$

to assess the effect of damping, the linear solutions without any dissipation were compared with the damped linear solutions based on the Rayleigh damping model. The comparison is presented in **Figures 8–11**, where the curves marked 2 (green) correspond to the linear solutions with Rayleigh damping.

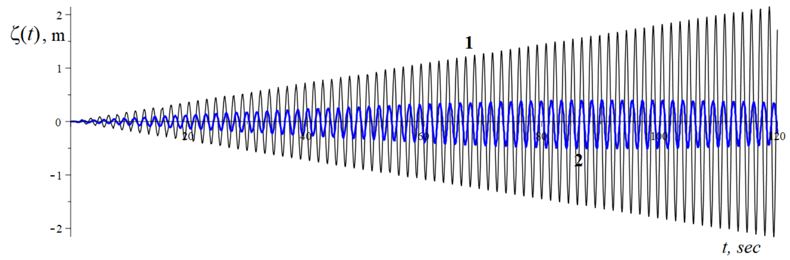

Figure 4. Free-surface elevation, loading Case A.

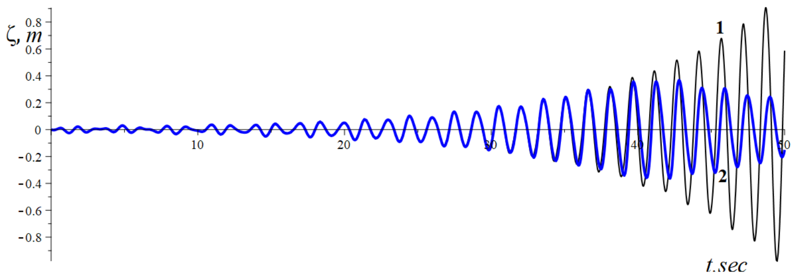

Figure 5. Free-surface elevation, loading Case B.

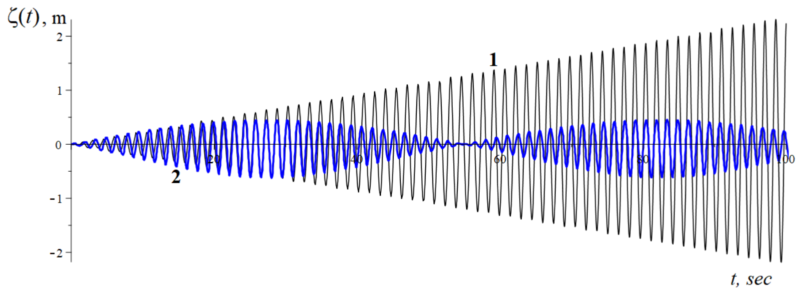

Figure 6. Free-surface elevation, loading Case C.

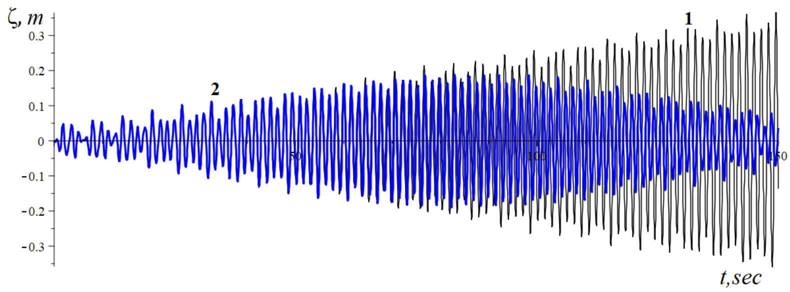

Figure 7. Free-surface elevation, loading Case D.

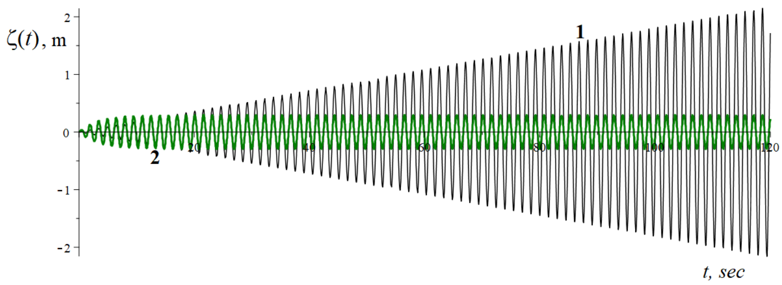

Figure 8. Free-surface elevation, loading Case A, including Rayleigh damping, $\xi = 0.05$.

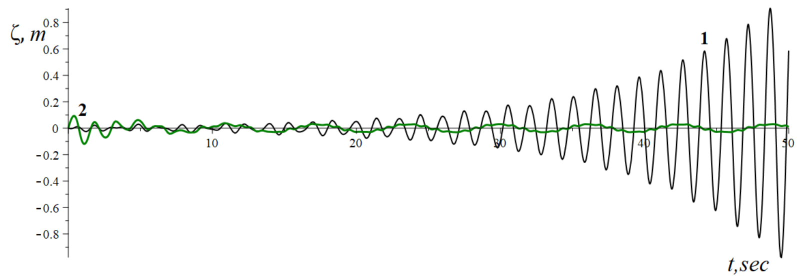

Figure 9. Free-surface elevation, loading Case B, including Rayleigh damping, ξ = 0.05.

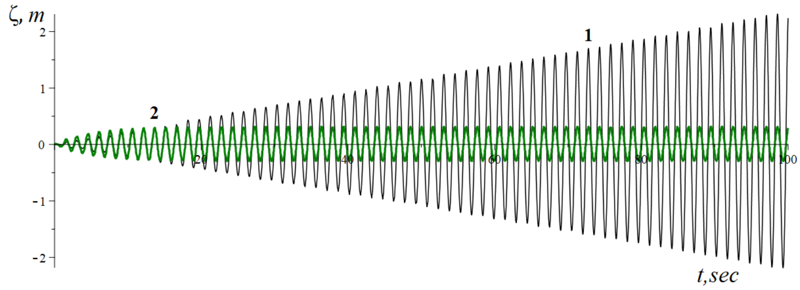

Figure 10. Free-surface elevation, loading Case C, including Rayleigh damping, ξ = 0.05.

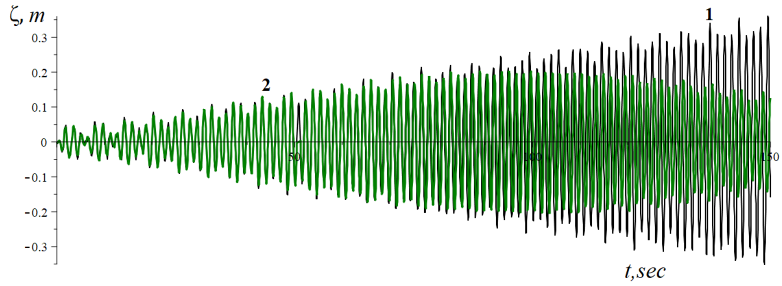

Figure 11. Free-surface elevation, loading Case D, including Rayleigh damping, ξ = 0.05.

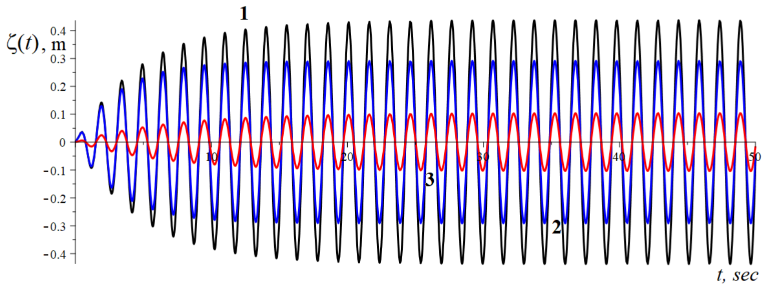

Figure 12. Comparison of liquid sloshing elevations in Case A for different Rayleigh damping ratios: ξ = 0.05 (black curve 1), ξ = 0.03 (blue curve 2), and ξ = 0.01 (red curve 3).

As expected, the amplitude decay rate increases with higher Rayleigh damping ratios. The case with ξ = 0.05 demonstrates the most pronounced damping effect, resulting in a significantly faster reduction of the sloshing amplitude. In contrast, reducing the damping ratio to 0.01 leads to only minor energy dissipation, preserving higher oscillation amplitudes even after a considerable number of periods. This behavior confirms the dominant role of the applied Rayleigh damping in controlling the numerical dissipation of the sloshing motion in the ideal fluid model.

Thus, numerical calculations are carried out for the free-surface elevation of a liquid in a cylindrical tank subjected to combined horizontal and vertical dynamic loads. The same problem was also solved with the inclusion of Rayleigh damping.

Both the fully nonlinear formulation and the Rayleigh-damped linear models lead to a clear reduction in the amplitude of sloshing oscillations. Consequently, the unphysical phenomenon of unbounded (infinitely growing) resonant amplitudes that appears in the purely linear undamped theory is completely eliminated in both approaches. For the specific loading conditions and geometry considered in this study, the nonlinear multimodal model yields results comparable to the conventional Rayleigh damping approach within the first 100–120 s of simulation, while providing additional physical insight into the softening behavior and energy transfer mechanisms.

However, the two methods differ fundamentally in their physical basis and long-term behaviour. Rayleigh damping is an empirical, phenomenological model in which energy dissipation is introduced artificially through mass- and stiffness-proportional terms; it is convenient for engineering calculations but lacks a direct link to the actual viscous or turbulent mechanisms inside the fluid. In contrast, the nonlinear formulation retains the full geometric and kinematic nonlinearities of the free-surface boundary conditions. These nonlinear terms naturally limit the oscillation amplitude through energy transfer to higher harmonics and self-limiting wave steepening, without any artificial dissipation. Consequently, the nonlinear solution exhibits bounded, non-decaying oscillations after the initial transient phase.

In several loading scenarios (most notably Cases A and D), the time histories and spatial patterns of sloshing obtained with the nonlinear model and with Rayleigh damping are similar for at least the first 70 s. This good short-term agreement confirms the validity of both approaches within the typical duration of many engineering transient events (e.g., seismic excitation), while highlighting that the nonlinear model offers a more physically consistent description for longer simulation times or for studies where artificial damping should be avoided.

So, these results demonstrate that proper inclusion of nonlinear free-surface effects can replace empirical damping models in many practical applications, providing a robust, energy-conserving description of resonant liquid sloshing in tanks.

9. Conclusion

The theoretical foundations for nonlinear modelling of liquid sloshing in tanks are developed using a spectral approach, together with methods for accounting for energy dissipation. A generalized formulation of the nonlinear free-surface hydrodynamic boundary-value problem is constructed, incorporating geometric and kinematic nonlinearities of the boundary conditions. It is shown that such a formulation is necessary for an adequate description of resonant sloshing regimes and for capturing amplitude limitation effects. A method for constructing basis functions based on the solution of the corresponding linear spectral boundary-value problem is proposed. The use of eigenmodes as a basis for representing the unknown functions is justified, as it ensures efficient dimensionality reduction and provides a clear physical interpretation of the generalized coordinates. A system of singular integral equations with 2π-periodic kernels is derived. The analytical properties of the integral operator kernels are investigated, establishing their regularizability and justifying the feasibility of an accurate numerical solution. A numerical approach for solving the system of singular integral equations is developed, ensuring convergence and stability of the computational process. It is demonstrated that the use of specialized quadrature schemes, together with proper treatment of kernel singularities, enables high accuracy of the results. A system of differential equations describing the linear formulation of the problem is constructed, and Rayleigh damping is introduced as a model for energy dissipation. It is shown that this approach is convenient for engineering estimates, although it has limited physical justification. A solvable system of differential equations for the nonlinear problem in generalized coordinates is formulated, accounting for modal interactions and enabling the description of complex free-surface dynamics, including energy transfer between harmonics. Based on a comparative analysis, it is established that Rayleigh damping provides a qualitatively correct description of oscillation decay over limited time intervals but does not reflect the actual physical dissipation mechanisms. The nonlinear model naturally limits oscillation amplitudes without introducing artificial damping, thereby providing a more physically consistent description of the sloshing process, although it does not inherently lead to amplitude decay.

It is acknowledged that the introduction of linear Rayleigh damping into an inviscid potential flow model is an engineering approximation. This term is intended to represent the cumulative dissipative effects of viscous boundary layers, weak wave breaking, and surface contamination. While fully nonlinear viscous CFD simulations provide a more physically consistent description of dissipation, they are computationally expensive for long-time simulations and parametric studies. The present modal approach with Rayleigh damping may provide a practical compromise for engineering applications.

In future work, the approach will be extended to shells of more general shapes, and the influence of internal baffles on sloshing dynamics will be investigated.

Author contributions: Conceptualization, ES and VG; methodology, VG; software programming, designing computer codes, DK; software testing and verification of the developed code, AK; validation, KD; formal analysis, DS; numerical research, KD; data curation, KD; writing—review and editing, AR; supervision, ES. All authors have read and agreed to the published version of the manuscript.

Funding: This work received no external funding.

Institutional review board statement: Not applicable.

Informed consent statement: Not applicable.

Data availability statement: The data supporting the numerical results of this study are available from the corresponding author upon reasonable request.

Conflict of interest: The authors declare no conflict of interest.

AI use statement: During the preparation of this manuscript, the authors used ChatGPT solely for language refinement. No AI tools were used for data analysis, interpretation, or generation of scientific content. The authors subsequently reviewed and edited the content as necessary and take full responsibility for the final content of the published article.

References

1. Ibrahim RA. Liquid Sloshing Dynamics: Theory and Applications, 1st ed. Cambridge University Press; 2005. doi: 10.1017/CBO9780511536656
2. Abramson HN, Chu WH, Ransleben GE. Representation of Fuel Sloshing in Cylindrical Tanks by an Equivalent Mechanical Model. ARS Journal. 1961; 31(12): 1697–1705. doi: 10.2514/8.5896
3. Faltinsen OM. A Nonlinear Theory of Sloshing in Rectangular Tanks. Journal of Ship Research. 1974; 18(04): 224–241. doi: 10.5957/jsr.1974.18.4.224
4. Liu Y, Wang J, Faltinsen OM, et al. Numerical prediction of wave loads and motions for ships with forward speed by a frequency-domain harmonic polynomial method. Ocean Engineering. 2026; 359: 125981. doi: 10.1016/j.oceaneng.2026.125981
5. Faltinsen OM, Rognebakke OF, Lukovsky IA, et al. Multidimensional modal analysis of nonlinear sloshing in a rectangular tank with finite water depth. Journal of Fluid Mechanics. 2000; 407: 201–234. doi: 10.1017/S0022112099007569
6. Faltinsen OM, Timokha AN. An adaptive multimodal approach to nonlinear sloshing in a rectangular tank. Journal of Fluid Mechanics. 2001; 432: 167–200. doi: 10.1017/S0022112000003311
7. Faltinsen OM, Timokha AN. Sloshing. Cambridge University Press; 2009.
8. Zang QS, Liu J, Zhang B, et al. Semi-analytical analysis of nonlinear liquid sloshing in rectangular tanks with scaled boundary finite element method. Physics of Fluids. 2024; 36(7): 075160. doi: 10.1063/5.0213683
9. Ikeda T, Ibrahim RA, Harata Y, et al. Nonlinear liquid sloshing in a square tank subjected to obliquely horizontal excitation. Journal of Fluid Mechanics. 2012; 700: 304–328. doi: 10.1017/jfm.2012.133
10. Gavrilyuk IP, Lukovsky IA, Timokha AN. Linear and nonlinear sloshing in a circular conical tank. Fluid Dynamics Research. 2005; 37(6): 399–429. doi: 10.1016/j.fluiddyn.2005.08.004
11. Lukovsky IA, Timokha AN. Multimodal Method in Sloshing. Journal of Mathematical Sciences. 2017; 220(3): 239–253. doi: 10.1007/s10958-016-3181-7
12. Chanto K, Pulngern T, Tangbanjongkij C, et al. Effect of Bending Rigidity and Nonlinear Strains on Free Vibration of Hemi-Ellipsoidal Shells. Journal of Vibration and Acoustics. 2023; 145(5): 051004. doi: 10.1115/1.4063114
13. Gani E, Öztürk S, Sari A, et al. Effects of Liquid Sloshing in Storage Tanks: An Overview of Analytical, Numerical, and Experimental Studies. International Journal of Steel Structures. 2025; 25(2): 544–556. doi: 10.1007/s13296-025-00946-8
14. Miliaiev A, Timokha A. Viscous damping of steady-state resonant sloshing in a clean rectangular tank. Journal of Fluid Mechanics. 2023; 965: R1. doi: 10.1017/jfm.2023.372
15. Konar T, Das A. A review of numerical modelling of liquid sloshing in partially filled containers. Ships and Offshore Structures. 2025; 1–26. doi: 10.1080/17445302.2025.2491080
16. Zhang Z, Tao A, Wu Q, et al. Review on the Progress and Issues in Liquid Tank Sloshing of Ships. China Ocean Engineering. 2023; 37(5): 709–724. doi: 10.1007/s13344-023-0060-0
17. Ma B, Yue B, Lu Y, et al. Numerical and experimental study on the nonlinear liquid sloshing in ellipsoidal tanks. Acta Mechanica. 2024; 235(9): 5545–5560. doi: 10.1007/s00707-024-04002-0
18. Cao Z, Xue MA, Fan H, et al. A semi-analytical study of nonlinear sloshing in a two-dimensional rectangular tank with a vertical baffle. Nonlinear Dynamics. 2025; 113(19): 25917–25944. doi: 10.1007/s11071-025-11442-3
19. Meng X, Sun Y, Wang J, et al. Nonlinear semi-analytical modeling of liquid sloshing in rectangular container with horizontal baffles. Applied Mathematics and Mechanics. 2023; 44(11): 1973–2004. doi: 10.1007/s10483-023-3054-8
20. Barik JR, Biswal KC. Nonlinear dynamic assessment of sloshing in a seismically isolated rectangular liquid tank using laminated rubber bearing. Soil Dynamics and Earthquake Engineering. 2024; 177: 108425. doi: 10.1016/j.soildyn.2023.108425

21. Roy SS, Biswal KC. Non-linear sloshing characteristics of liquid inside a chamfered bottom tank with submerged internal object under near-and far-fault earthquakes. Ocean Engineering. 2024; 309: 118593. doi: 10.1016/j.oceaneng.2024.118593
22. Yang C, Ni H, Liu J, et al. The effect of the stiffeners of the external-pressure tank in a buoyancy regulator on the inside liquid sloshing. Engineering Computations. 2025; 42(3): 1122–1138. doi: 10.1108/EC-05-2024-0403
23. Hu Q, Liu S, Zhang K, et al. Experimental and Numerical Investigation of Stiffness-Optimized Vibration Isolators on Vibration Transmission in Cylindrical Shell Structures: A Comparative Land-Based and Underwater Study. Vibration. 2026; 9(2): 31. doi: 10.3390/vibration9020031
24. Barik JR, Biswal KC. Nonlinear Seismic Response of a Base-Isolated Liquid Container Having a Bottom-Mounted Submerged Internal Block. Journal of Earthquake Engineering. 2026; 1–41. doi: 10.1080/13632469.2026.2650345
25. Brietman NL, Bar-Yoseph PZ, Suponitsky V. Nonlinear liquid sloshing dynamics: Post-processing of conventional finite element solutions by digital filters. Ocean Engineering. 2022; 249: 110837. doi: 10.1016/j.oceaneng.2022.110837
26. Limarchenko OS, Nefedov AA, Semenovich EA. Manifestation of Secondary Resonances during Pendulum Vibrations of a Tankwith Fluid. International Applied Mechanics. 2020; 56(6): 741–749. doi: 10.1007/s10778-021-01051-z
27. Yoshitake T, Ishikawa S, Kondou T. Analysis of two-dimensional nonlinear sloshing in a rectangular tank by using a concentrated mass model. Journal of Vibration and Control. 2023; 29(15–16): 3418–3434. doi: 10.1177/10775463221095934
28. Bykov Y, Khoryev O, Korotaiev P, et al. Numerical Investigation of Unsteady Flow in Draft Tube with Ribs. In: Proceedings of the 2022 IEEE 3rd KhPI Week on Advanced Technology (KhPIWeek); 3–7 October 2022; Kharkiv, Ukraine. pp. 1–6. doi: 10.1109/KhPIWeek57572.2022.9916461
29. Smetankina N, Merkulova A, Merkulov D, et al. Modelling Thermal Stresses in Laminated Aircraft Elements of a Complex Form with Account of Heat Sources. In: International Conference on Reliable Systems Engineering (ICoRSE)—2022. Springer International Publishing; 2022. pp. 233–246. doi: 10.1007/978-3-031-15944-2_22
30. Vorobiov IS, Chugay MO, Rao JS, et al. Analysis of turbomachinery blading vibrations using new materials. Journal of Vibration Engineering and Technologies Open Source Preview. 2014; 2(6): 529–535. Available online: https: //www.researchgate.net/publication/279324048
31. Ma B, Yue B. Arbitrary Lagrangian-Eulerian finite element method for liquid sloshing with contact angle hysteresis in microgravity. Advances in Space Research. 2025; 75(1): 1585–1596. doi: 10.1016/j.asr.2024.11.043
32. Choudhary N, Degtyarev K, Kriutchenko D, et al. Shell-like structures interacting with liquids and their applications. Journal of Applied Mathematics and Mechanics. 2025; 105(9): e70227. doi: 10.1002/zamm.70227
33. Gnitko V, Degtyariov K, Naumenko V, et al. BEM and FEM Analysis of the Fluid-Structure Interaction in Tanks With Baffles. International Journal of Computational Methods and Experimental Measurements. 2017; 5(3): 317–328. doi: 10.2495/CMEM-V5-N3-317-328
34. Ugrimov S, Smetankina N, Kravchenko O, et al. A Study of the Dynamic Response of Materials and Multilayer Structures to Shock Loads. In: Advances in Mechanical and Power Engineering, Lecture Notes in Mechanical Engineering. Springer International Publishing; 2023. pp. 304–313. doi: 10.1007/978-3-031-18487-1_31
35. Raynovskyy I, Timokha A. Steady-State Resonant Sloshing in an Upright Cylindrical Container Performing a Circular Orbital Motion. Mathematical Problems in Engineering. 2018; 2018: 1–8. doi: 10.1155/2018/5487178
36. Fang X, Bao X, Yue F, et al. A Dynamic Analysis Method of Liquid-Filled Containers Considering the Fluid–Structure Interaction. Applied Sciences. 2024; 14(7): 2688. doi: 10.3390/app14072688
37. Avramov K, Uspensky B, Liubarskyi B. Asymptotic analysis of resonant nonlinear oscillations of composite sandwich doubly curved shell with soft honeycomb core under axial harmonic excitation. Acta Mechanica. 2026; doi: 10.1007/s00707-026-04648-y
38. Sierikova O, Strelnikova E, Gnitko V, et al. BoundaryCalculation Models for Elastic Properties Clarification of Three-dimensional Nanocomposites Based on the Combination of Finite and Boundary Element Methods. In: Proceedings of the 2021 IEEE 2nd KhPI Week on Advanced Technology (KhPIWeek); 13–17 September 2021; Kharkiv, Ukraine. pp. 351–356. doi: 10.1109/KhPIWeek53812.2021.9570086
39. Lukovsky IA. Nonlinear Dynamics: Mathematical Models for Rigid Bodies with a Liquid. DE GRUYTER; 2015. doi: 10.1515/9783110316575
40. Brebbia CA, Telles JCF, Wrobel LC. Boundary Element Techniques. Springer; 1984. doi: 10.1007/978-3-642-48860-3

41. Karaiev A, Strelnikova E. Singular integrals in axisymmetric problems of elastostatics. International Journal of Modeling, Simulation, and Scientific Computing. 2020; 11(01): 2050003. doi: 10.1142/S1793962320500038
42. Strelnikova E, Choudhary N, Degtyariov K, et al. Boundary element method for hypersingular integral equations: Implementation and applications in potential theory. Engineering Analysis with Boundary Elements. 2024; 169: 105999. doi: 10.1016/j.enganabound.2024.105999
43. Kovacic I, Rand R, Mohamed Sah S. Mathieu's Equation and Its Generalizations: Overview of Stability Charts and Their Features. Applied Mechanics Reviews. 2018; 70(2): 020802. doi: 10.1115/1.4039144
44. Habenberger J. Fluid damping of cylindrical liquid storage tanks. SpringerPlus. 2015; 4(1): 515. doi: 10.1186/s40064-015-1302-2
45. Yang H, Purandare R, Peugeot J, et al. Prediction of Liquid Slosh Damping Using a High Resolution CFD Tool. In: Proceedings of the 48th AIAA/ASME/SAE/ASEE Joint Propulsion Conference & Exhibit; 30 July–1 August 2012; Atlanta, GA. doi: 10.2514/6.2012-4294
46. Rossetti F, Pirillo L, Cimini M. et al. Numerical Investigation on the Liquid Sloshing Damping inside a Tank with a Flexible Anti-Sloshing Device. In: Proceedings of the 34th Congress of the International Council of the Aeronautical Sciences ICAS 2024; 9–13 September 2024; Florence, Italy. Available online: https://www.icas.org/icas_archive/icas2024/data/papers/icas2024_0930_paper.pdf
47. Lukovsky I, Ovchynnykov D, Timokha A. Asymptotic nonlinear multimodal modeling of liquid sloshing in an upright circular cylindrical tank. I. Modal equations. Nonlinear Oscillations. 2012; 14(4): 512–525. doi: 10.1007/s11072-012-0173-5
48. Solodun AV, Timokha AN. The Narimanov–Moiseev Multimodal Analysis of Nonlinear Sloshing in Circular Conical Tanks. In: Applied Mathematical Analysis: Theory, Methods, and Applications, Studies in Systems, Decision and Control. Springer International Publishing; 2019. pp. 267–309. doi: 10.1007/978-3-319-99918-0_9
49. Liang H, Santo H, Shao Y, et al. Liquid sloshing in an upright circular tank under periodic and transient excitations. Physical Review Fluids. 2020; 5(8): 084801. doi: 10.1103/PhysRevFluids.5.084801
50. Liu R, Shao Y, Chen J, et al. Nonlinear liquid sloshing in an upright circular container: Modal responses and higher-order harmonics. Physics of Fluids. 2022; 34(1): 012116. doi: 10.1063/5.0077206